Tellus (1989), *41A*, 162–174

Surface currents in the Norwegian Channel measured by radar in March 1985

By HEINZ-HERMANN ESSEN, KLAUS-WERNER GURGEL and FLORIAN SCHIRMER,
Institut für Meereskunde, Universität Hamburg, Troplowitzstrasse 7, D-2000 Hamburg 54, FRG

(Manuscript received 26 January 1987; in final form 22 February 1988)

ABSTRACT

Surface currents, as measured by a land-based HF radar (CODAR), are presented. The experiment was carried out in the Norwegian Channel (59° N) from March 12 to 22, 1985. Two-dimensional surface currents were mapped every 2 h, or 1 h during periods of strong wind. The current shows a strong variability on small horizontal (several km) and short temporal (days) scales, containing a large amount of energy. The development of eddies could be studied, which rotated anticlockwise with velocities up to 80 cm s^{-1} and remained stable for about one day. From time series at different positions, the semidiurnal tide and the wind-driven part of the current is estimated. The tidal currents confirm with already-known results. The ratio of current-to-wind velocity (0.019 and 0.010, for the north- and east-components, respectively) are derived from surface currents directly and may be more reliable than other estimates. The horizontal curl and divergence are calculated and presented for one grid point. Both the curl and divergence change sign several times during the experiment. The curl shows a 2-day period of high rotation; and a two-day period of upwelling could also be observed. Absolute values of the linear (local) and nonlinear (advective) acceleration are compared. For tidal motions, the linear terms exceed the nonlinear, but generally, this is not the case for currents on the considered scales.

1. Introduction

Mesoscale processes, like eddies of diameters between 10 km and 100 km, gain more and more interest in oceanographic research. Eddies of this scale mainly occur in coastal regions or in the marginal ice zone. they affect man's activities like shipping, fishing, engineering and the distribution of polluted water masses. They also influence the large-scale circulation in the ocean, or the retreat and advance of the ice edge.

The eddy dynamics, such as generation, propagation and decay is not yet understood, nor is its influence on the large-scale circulation. Numerical circulation models are usually wind-driven, while measurements in the North Sea also show a strong non-wind-driven component. Beside density effects, mesoscale processes have to be taken into account. In order to parameterise these processes, a better understanding of eddy dynamics is desired. Extensive experimental and theoretical studies are necessary.

Ship surveys are the classical tool of oceanographers to study processes like eddies. For about 20 years, remote sensing methods have become more and more important. Their main advantage is the synoptic view of the ocean. Electromagnetic methods are restricted to the surface of the ocean. Well-known are the infrared satellite photos. Acoustic waves are appropriate to observe the inner ocean, and some success is made in deep water (acoustic tomography), but it is questionable, whether these methods will ever work in shallow water.

Beside the air-borne electromagnetic remote sensing methods which work with wavelengths less than 10 cm, HF (high frequency) methods are available to observe the ocean from land (or from board a platform or ship). The wavelengths used, from 10 m to 100 m, correspond to the wavelengths of surface waves. Ocean waves themselves and surface currents, carrying the waves, may be measured remotely by this method.

The use of HF radar systems offers a unique method of measuring mesoscale current fields, which are hard to measure by conventional means. Moored current meters cannot be operated close to the sea surface, because the records are distorted by the action of surface waves. CODAR (Coastal Radar), originally developed by Barrick et al. (1977), is able to map surface currents in the upper 1 m of the ocean. An area of some 40 km × 40 km may be covered with a spatial resolution of about 2 km. The current velocities are available on a two-dimensional grid system, and are thus very appropriate for comparison with the results of numerical models.

The measuring system is based on the backscatter of transmitted CW (continuous wave) pulses from the moving rough sea surface. The Doppler shift determines the phase velocity of the scattering surface waves. In the absence of currents, this phase velocity is theoretically known. Differences between measured and predicted phase velocity are due to underlying currents. One radar station measures the radial current velocity with respect to its site. Two stations, separated by some 30 km, are necessary to determine the two-dimensional current vectors. A more detailed description of the CODAR, operated by the University of Hamburg (FRG) is given elsewhere (Essen et al., 1983 and 1984).

In March 1985, the Institute of Oceanography (University of Hamburg) carried out an experiment in the Norwegian Channel, between 59° N and 60° N. The objective was to study the three-dimensional variability within the Norwegian Coastal Current during early spring. The research vessel VALDIVIA of the University of Hamburg served as a platform for deploying water-level recorders across the trench and mapping the three-dimensional structure of the circulation system by use of a towed profiler, measuring temperature and salinity at different depths. Temporal resolution was achieved by repeated hydrographic sections.

The hydrographic survey from on board VALDIVIA was supplemented by land-based CODAR measurements, yielding the two-dimensional surface currents. This paper reports the remotely-measured current fields, only. They show a very complex spatial and temporal behaviour.

2. The Norwegian coastal current

The currents within the measuring area are dominated by the Norwegian coastal current, which follows the west coast of Norway and flows, on the average, northward. It carries the main transport of water masses out of the North Sea into the Atlantic. The Norwegian coastal current is conducted by the trench in front of the Norwegian coast, which is relatively narrow (~100 km). There is a very distinct frontal structure between the cold northward flowing coastal water of low salinity and the warmer Atlantic water of higher salinity in the inner North Sea. This front shows a strong temporal and spatial variability with scales from some 10 km up to 100 km. The Norwegian coastal current has been studied extensively in the past 15 years. This applies to conventional hydrographic measurements as well as to infrared imagery from satellites and theoretical investigations.

During the Joint North Sea Data Acquisition Program in spring 1976 (JONSDAP 1976), four moorings of 4 or 5 current meters, each, were operated across the Norwegian Trench at the latitude of Utsira. The data were analysed with respect to the transport rates through the trench and the influence of the wind (Furnes and Saelen, 1977, Furnes, 1981, Dooley and Furnes, 1981). It turned out that the main transport out of the North Sea is the Norwegian coastal current. The fluxes undergo strong temporal variations which may be related to the wind field over the North Sea. These experimental results are corroborated by a simple rectangular numerical model of the North Sea, which shows that the presence of a trench can cause a wind-driven flow to pass it (Davies and Heaps, 1980). The JONSDAP data were also used to determine the semidiurnal tide and to compare it with results of a numerical model (Davies and Furnes, 1980).

The frontal structure of the Norwegian coastal current becomes clearly visible in satellite infrared images (Audunson et al., 1981, Johannessen et al., 1983, Carstens et al., 1984). These images show the spatial distribution of sea surface temperatures, but contain no information about current speeds. Waves with wavelengths of some 100 km and amplitudes up to 50 km exist at the front; eddies of 50 km diameter can be observed. But there is also a high variability on smaller scales between 10 km and 50 km within the coastal current, sometimes very close to the coast. Experiments in a rotating basin yielded similar features (Vinger et al., 1981), as observed at the edge of the Norwegian coastal current. The existence of meanders or decay into eddies turned out to be strongly dependent on the velocity of the current regimes.

Recently, the simple picture of an isolated Norwegian coastal current undergoes some modifications. From biological and current meter observations, Furnes et al. (1986) conclude on the existence of a cross-trench circulation of Atlantic water, which is strongly affected by short-term (days) variations. In particular, the instability of the front is mentioned, which results in meanders and eddies.

3. CODAR measurements

Two CODAR stations were deployed on the Norwegian island Utsira (59°17.70′N, 4°53.42′E) and the peninsula Karmoy (59°10.95′N, 5°10.95′E), approximately 21 km apart. Each station consisted of the nearly omnidirectional transmitting antenna (with slight directivity towards the sea) and an array of four receiving antennas. At both stations, the antennas were mounted on top of rocks, approximately 10 m above the sea surface, allowing an angle of sight of nearly 180°. The data-processing was performed on-line, i.e., each station yielded the radial current velocities after 60 min of processing time.

In general, the maximum range of the Utsira station was about 35 km, that of the Karmoy station about 40 km. The difference is probably due to a number of rocks, standing out of the water in front of the Utsira station, or to the cable connection between antennas and radar receiver. At both stations, long cables were necessary, some 100 m for Karmoy and some 150 m for Utsira. This may also be the reason for the smaller range as compared with experiments from the German island of Sylt (Essen et al., 1983).

The experiment was performed from 12 March, 11.00 GMT until 23 March, 7.00 GMT, 1985. The measuring interval was 2 h during the whole time and 1 h during periods of increasing winds (12 March, 21.00 GMT until 14 March, 11.00 GMT, and 20 March, 17.00 GMT until 22 March, 1.00 GMT). Due to system failures, four measurements are missing in this scheme. In total, 150 current maps are available.

The measured current velocities represent temporal and spatial averages. The temporal averaging is determined by the record length of 18 min, the spatial averaging mainly by the transmitted pulse length of 16 μs, and is some 10 km². CODAR measures the current down to about 0.5 m. There is no other system, measuring exactly the same quantity as CODAR does. Thus, an estimation of accuracy by comparing with other measurements is not possible. Standard deviations, gained from averaging within the data processing algorithms, provide a reliability of about 2 cm s⁻¹ for mean radial current

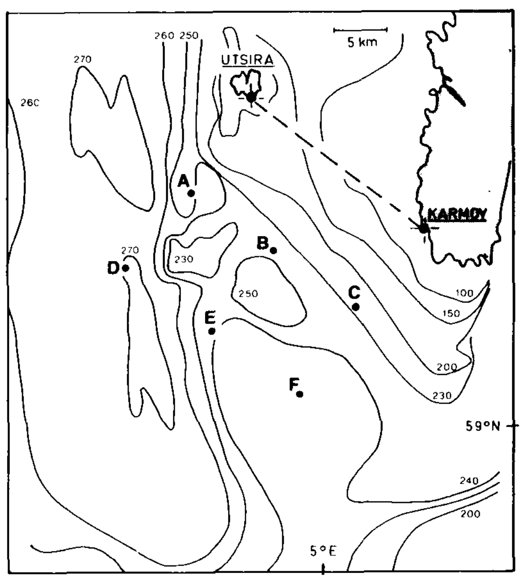

Fig. 1. Topography and bathymetry of the measuring area. The radar sites are marked by points and connected by the dashed baseline. The locations A–F are referred to in later figures. The contours are given in metres.

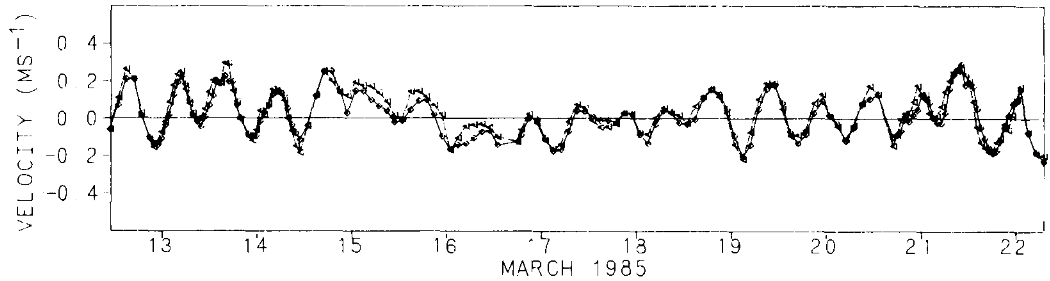

Fig. 2. Comparison of radial current velocities on the baseline (cf. Fig. 1), where both stations measure the same value. The current velocities refer to the centre of the baseline.

velocities, as used for constructing the two-dimensional vectors.

Fig. 1 shows the topography and the bathymetry of the measuring area. The two radar stations are marked by crosses. The letters A–F indicate locations to which we will refer later. The deployment of the CODAR systems on islands allowed the comparison of both stations. Fig. 2 shows radial current velocities as measured in the centre of the baseline, connecting both stations (dashed line in Fig. 1). Usually, the baseline coincides with the coastline and no comparison is possible.

The current velocities in Fig. 2 represent mean values within a circle of 3 km radius. Obviously, the agreement is excellent. The small phase shift between the time series is due to the fact that the measurements were carried out successively in order to avoid interferences, but plotted for full hours.

4. Two-dimensional current velocities

In order to determine the horizontal current field, a grid system is defined. Radial current velocities, measured within a certain circle around each grid point, are averaged. The two-dimensional current vector is combined from the mean radial components of the two radar stations. For the presentation in this paper, we used a grid distance of 3 km, and an averaging radius of 3 km. These values yield overlapping averages, i.e., current velocities on adjacent grid points are dependent on each other. In cases of right angles or nearly right angles between the radial components, 2 cm s^{-1} can be accepted as a reasonable error for both components of the two-dimensional vector. The more the angle deviates from 90°, the larger becomes the error of at least one component. On the baseline, no two-dimensional vector can be determined. Moreover, if the standard deviation of one of the mean radial velocities exceeds 25 cm s^{-1}, no vector is plotted.

From the 150 current maps of the experiment, we can present only some examples in Figs. 3–5. All available current fields show strong horizontal variabilities. The four successive current maps from 12 March in Fig. 3, the first of the experiment, represent the usual situation. The turning of the tide is obvious and in this connection, eddy-like structures occur with diameters of some 10 km. These eddies have low velocities (about 10 cm s^{-1}) and rotate in different directions. Though they are not visible in all current maps, they may be present and covered by higher velocities.

Fig. 4 shows the beginning of an exceptional period during the experiment on 16 March. The interval between the maps is 6 h. On the first two maps, there are two flows directed to the southeast and north, respectively. The front between develops into a strong eddy of about 20 km diameter rotating anticlockwise. The eddy remains stable for about 24 h, its centre is moving to the southeast for about 5 km and then back to the northeast, obviously carried by the tides. Thereafter, it decays into a strong front, as shown by the successive maps of Fig. 5. Again, the frontal structure remains visible for another 24 h.

In Fig. 6, we show time series of the wind vector and surface current velocities at two different positions. The wind was measured by the

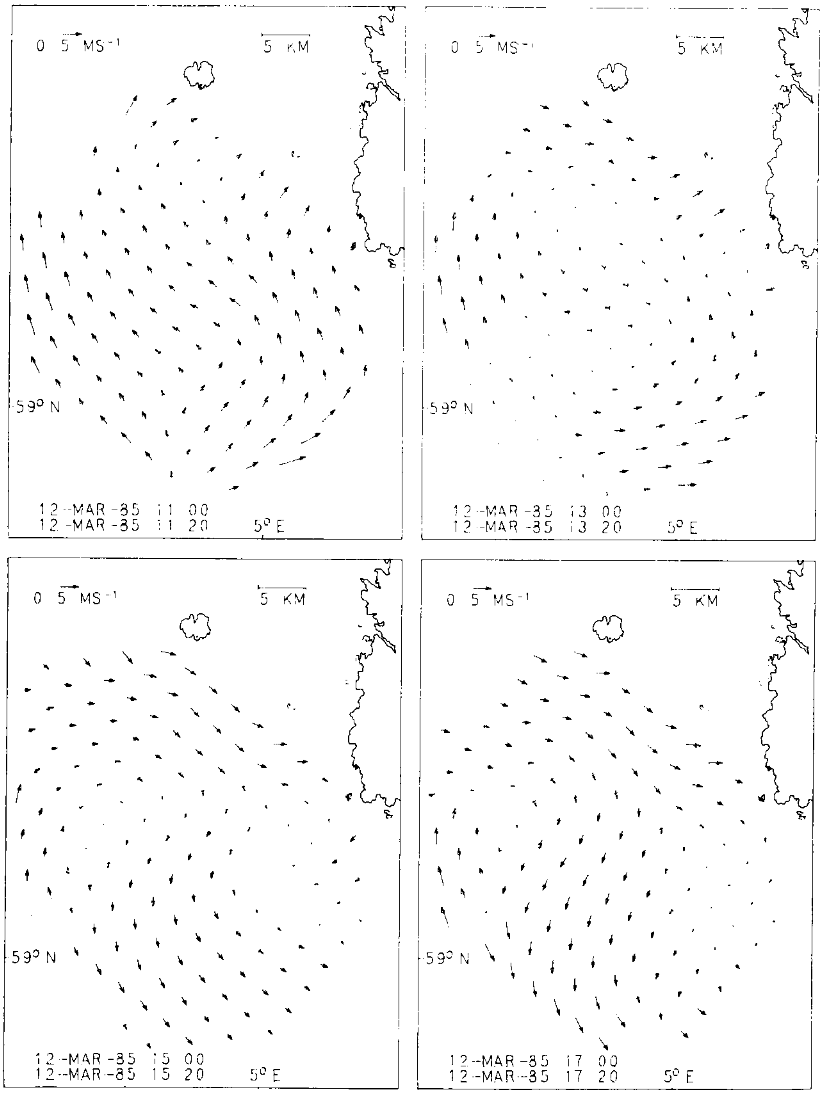

Fig. 3. Four successive current maps with 2 h sampling (normal situation). The times are in GMT.

weather station Utsira, close to the CODAR station (position given above). The wind changed considerably in speed as well as in direction. The first three days of the experiment (12–15 March) were characterized by strong winds of up to 12 m s^{-1}, rotating from south to west, decaying and blowing from west again. After a period of relative low winds (16–18 March), the wind increased again to speeds of 12 m s^{-1} on March 20, this time from the east.

The current vectors of Fig. 6 are obtained by the same procedures as those of the maps in Figs. 3–5. For the two positions (marked by B and F in Fig. 1), data are available for nearly all measurements. Though the positions are separated by only 14 km, the time series show significant differences. This applies mainly to the period from 16–17 March, where there was an eddy with position B close to its centre and position F at its edge (cf. Fig. 4). At both positions, the time

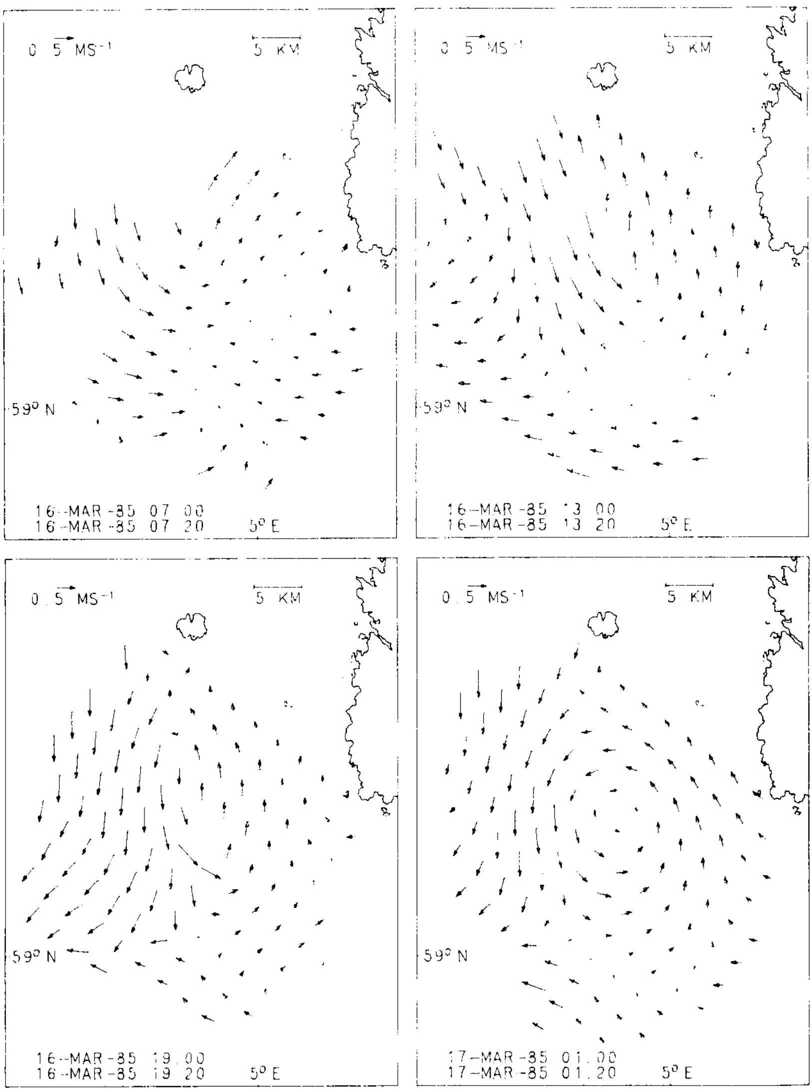

Fig. 4. Four current maps with 6 h sampling (development of an eddy). The times are in GMT.

series show a strong semidiurnal component (especially the north component). There is some resemblance between the wind and current vector, which however, is not always apparent, indicating other influences like eddies, fronts, and residual currents.

The eddy occurred after the wind had broken down. Also during its decay, the wind changed, but not that obviously. The eddy developed from a front, similar to the tank experiment of Vinger et al. (1981). But it also decayed into a front, with stronger gradient after the eddy period than before. The situation observed is different from the tank experiment. The front occurred within the coastal current and not at its edge, and it was of limited range. Beside the wind, the topography obviously influenced the eddy in restraining its motion.

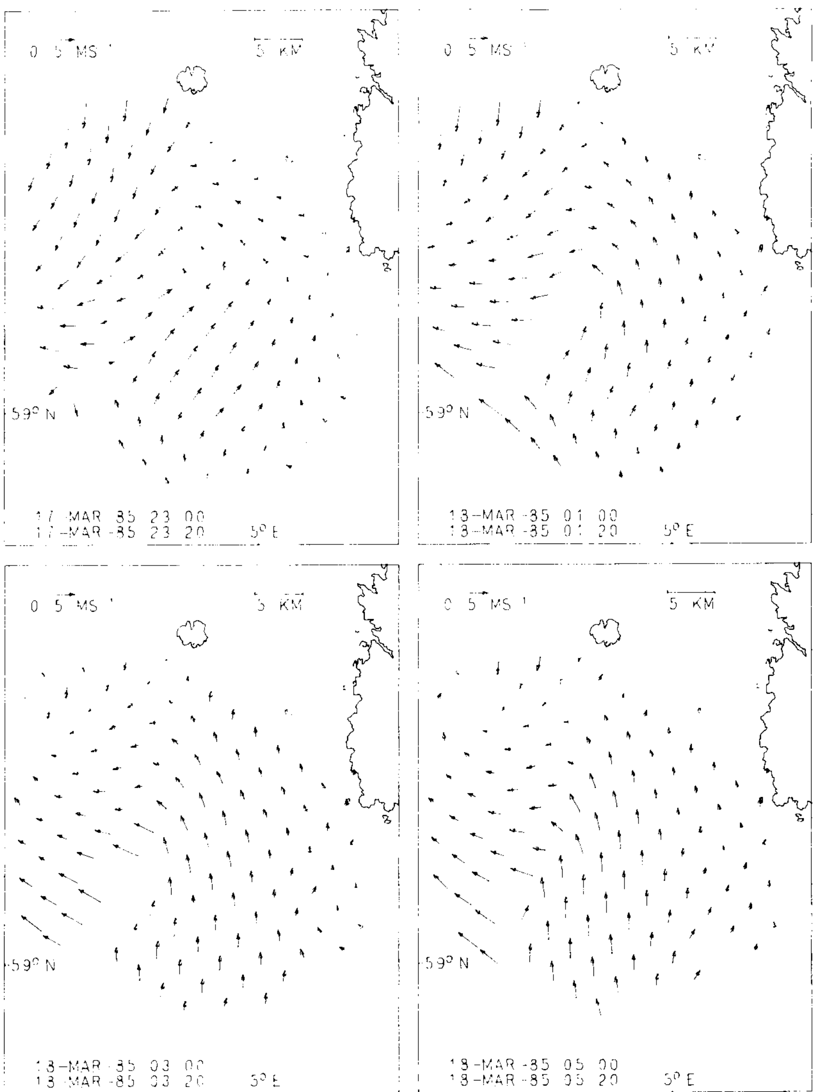

Fig. 5. Four successive current maps with 2 h sampling (development of a front). The times are in GMT.

5. Wind-driven and tidal parts of the current

The time series allow the estimation of the tidal and wind-driven parts of the currents. For this purpose, we tried to fit the measured current velocities with a number of sinusoidal tidal components and a function proportional to the observed wind. With the assumption of deviating surface current and wind direction, the fit could not be improved. It turned out that the data allow us to determine the mean semidiurnal tide of 12.4 h period, only. A least-squares fit was performed for the north- and east-component separately,

$$\sum_i \{u(t_i) - u_0 - a_T \times \cos\left(\frac{2\pi}{T} t_i - \phi_T\right) - \alpha w(t_i)\}^2 = \text{minimum}, \quad (1)$$

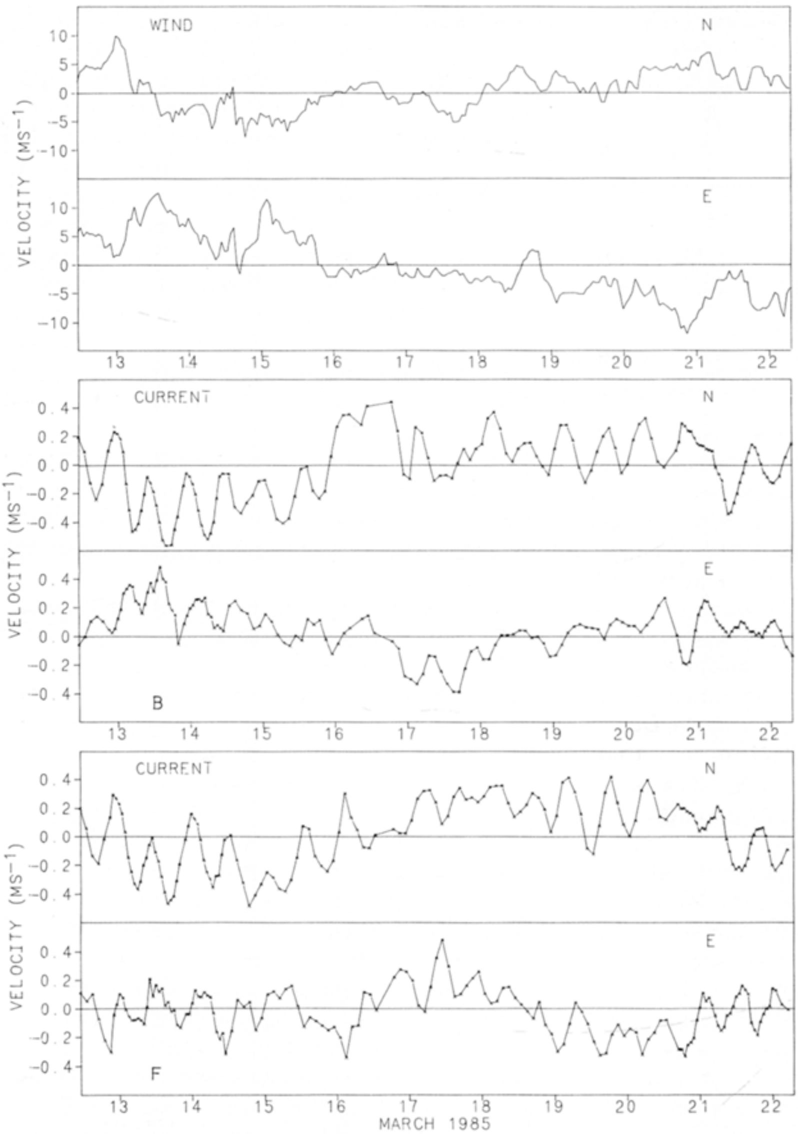

Fig. 6. Time series of the wind- and current-vector (N = north-, E = east-component), with wind from Utsira and currents at two different positions B and F of Fig. 1.

$u(t_i)$ = measured current velocity at times t_i (east or north component),
u_0 = mean (residual) current velocity,
a_T, ϕ_T = tidal amplitude and phase, respectively,
T = tidal period (12.4 h),
α = ratio of current-to-wind velocity,
$w(t_i)$ = observed wind velocity (east or north component) (with wind corrected to 10 m above sea level).

The method is described in more detail by Essen et al. (1983). The least-squares fit was carried out for the six positions A–F of Fig. 1. The results show some variation, due to perturbations like eddies and fronts, and also due to the influence of the coast. McClimans and Lonseth (1985) show that the presence of a front may amplify tidal motions, observed by single-point (Eulerian) current measurements. In order to suppress this effect and estimate its importance, we present the mean values over the six positions and their standard deviations:

residual currents

$$u_0 = \begin{cases} (-0.05 \pm 0.05)\ \mathrm{m\ s^{-1}} & \text{(north component)} \\ (0.02 \pm 0.04)\ \mathrm{m\ s^{-1}} & \text{(east component);} \end{cases}$$

tidal amplitudes and phases

$$a_T = \begin{cases} (0.12 \pm 0.02)\ \mathrm{m\ s^{-1}} & \text{(north component)} \\ (0.04 \pm 0.01)\ \mathrm{m\ s^{-1}} & \text{(east component);} \end{cases}$$

ratio of current-to-wind speed

$$\alpha = \begin{cases} 0.019 \pm 0.05 & \text{(north component)} \\ 0.010 \pm 0.05 & \text{(east component);} \end{cases}$$

The residual currents computed by this method do not include the influence of the local wind and should confirm the general features of the transport through the trench, as presented in Section 2. Unfortunately, the values of the residual currents show strong relative variations, and no conclusions are possible. As may be seen more clearly from the 25-h mean values, presented later, this is mainly due to the disturbance of the eddy period. The semidiurnal tidal ellipse agrees nearly exactly with that observed by Davies and Furnes (1980) during JONSDAP '76 at position 63, about 40 km west of Utsira. The ellipse at position 63, only a few kilometres north of Utsira and closer to our measuring area, is much narrower. But at position 63, the water depth is only some 100 m as compared to more than 200 m in our measuring area and at position 64.

The ratio of current-to-wind speed is of special interest, because of the available surface currents. Other estimations are based on current meter or drifter measurements. Current meters may be operated several metres below the surface only, and drifters may be directly influenced by the wind, yielding too high velocities. Pond and Pickard (1978) declare a ratio of current-to-wind speed of 0.014 for the latitude considered. This value refers to deep-water and steady-wind conditions, requirements which are not fulfilled by our experiment. Otherwise, the given value does not include the wave-induced Stokes drift, which is present in the CODAR data and may be of the same magnitude. Audunson et al. (1981) observed drift factors of about 2.5% of the wind velocity. The drifters floated in the upper 30 cm of the Norwegian coastal current at about 65° N.

The CODAR data yield a significant correlation between current and wind with a ratio nearly twice as high for the north as for the east component. This may be explained by the influence of the coast. Winds blowing from the east have only a small fetch and westward directed currents are restrained. The observed ratio of current-to-wind speed of the north component is between both the values mentioned above; that of the east component is lower. For both components, nearly the same ratios were observed east of the German island Sylt, in the southern North Sea (Essen et al., 1984). The distance from the coast was the same as in the Norwegian Trench, but the water depth is only 20 m in that area.

Davies (1985) presents numerical results (linear model) of wind-driven surface currents and shows the strong influence of eddy viscosity. For a wind speed of 22 m s^{-1} and eddy viscosities between 50 cm^2 s^{-1} and 4000 cm^2 s^{-1}, the ratio of current-to-wind speed varies between 0.06 and 0.006, with a value of 0.02 for the most appropriate eddy viscosity of 500 cm^2 s^{-1}. The numerical model differs in some aspects from our experiment. The wind arises suddenly and remains uniform at higher velocity as observed, and an open ocean is considered. Nevertheless, some conclusions may be drawn. Considering the eddy viscosity of 500 cm^2 s^{-1}, the ratio of current-to-wind speed agrees with our observation, and the numerical values are nearly the same for the investigated water depths of 35 m and 260 m (also in agreement with our observations). After the sudden imposition of the wind, the current follows its direction for about the first two hours. This and the unsteady wind conditions during the experiment may be the reason that we could observe no deviation between wind and current direction.

Figs. 7–8 compare mean values of the wind and current vector at the 6 positions A–F of Fig. 1. The averages were taken over 25 h in order to suppress the semidiurnal tide of 12.4-h period. Lacking data in the time series, due to missing measurements or too low range for some times and positions, are replaced by means of a cubic spline interpolation. Again, these figures show the high spatial and temporal variability for small (several kilometres) and short (days) scales, respectively. The mean currents are different at the 6 positions. This mainly applies to the eddy period on March 16–17, where the mean currents

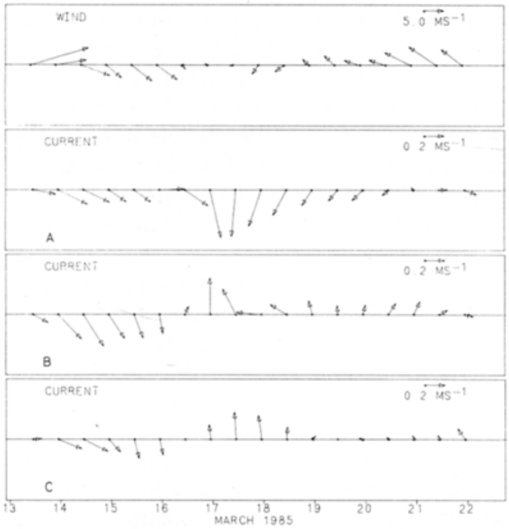

Fig. 7. 25-hourly means of the wind and current vector at positions A–C of Fig. 1 (north = upward, east = to the right).

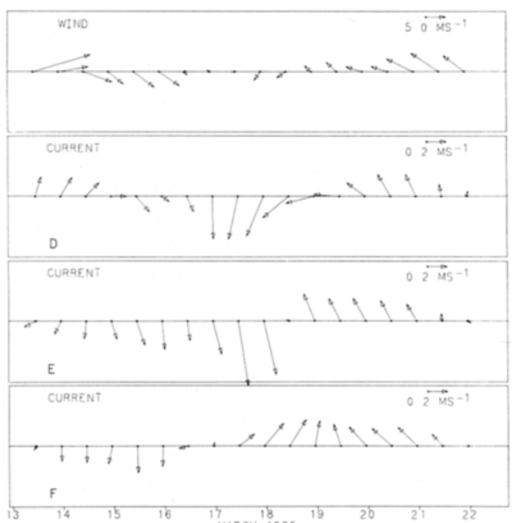

Fig. 8. 25-hourly means of the wind and current vector at positions D–F of Fig. 1 (north = upward, east = to the right).

at some positions become very high. But also for the other periods, there are significant differences, indicating the presence of mesoscale variabilities like eddies for the whole experiment.

6. Horizontal derivatives of current velocities

The two-dimensional current vectors presented so far are composed from two mean radial current velocities, as obtained from both radar stations within a circle around the considered grid point. Another method is to approximate the two components of the current vector by polynomials of first order.

$$\boldsymbol{u} = (u_x, u_y) \qquad (2)$$

$$u_x = a_1 + a_2 x + a_3 y \quad \text{(east component)},$$

$$u_y = a_4 + a_5 x + a_6 y \quad \text{(north component)},$$

The coefficients a_i are determined by means of least-squares fits from the radial currents of the two radar stations. With respect to the two-dimensional current vectors, both methods yield the same results. The advantage of the polynomial approach is that the horizontal derivatives of the currents may be determined. In principle, this should be possible from the current maps, too. But in cases of small differences, the results become numerically unstable. The polynomial approach is more accurate because it considers the range dependence of radial velocities also within the averaging circle.

The derivatives of eq. (2) allow the determination of the horizontal divergence and curl and the nonlinear acceleration:

$$\text{div}\, \boldsymbol{u} = \frac{\partial u_x}{\partial x} + \frac{\partial u_y}{\partial y} \quad \text{(horizontal divergence)}$$

$$\text{curl}\, \boldsymbol{u} = \frac{\partial u_y}{\partial x} - \frac{\partial u_x}{\partial y} \quad \text{(horizontal curl)} \qquad (3)$$

$$\boldsymbol{b}_h = (b_x, b_y), \quad \text{(advective acceleration)}$$

$$b_x = u_x \frac{\partial u_x}{\partial x} + u_y \frac{\partial u_x}{\partial y}, \quad b_y = u_x \frac{\partial u_y}{\partial x} + u_y \frac{\partial u_y}{\partial y}.$$

Another advantage of the least-squares fit is the possibility of estimating the errors of the current vector and its derivatives from the standard deviations of the radial current velocities by means of the respective covariance matrices. With respect to the current velocities, the same errors are obtained as stated above.

Fig. 9 shows the time series of the curl and divergence at the position B of Fig. 1. In order to obtain numerically stable values for all 150 mea-

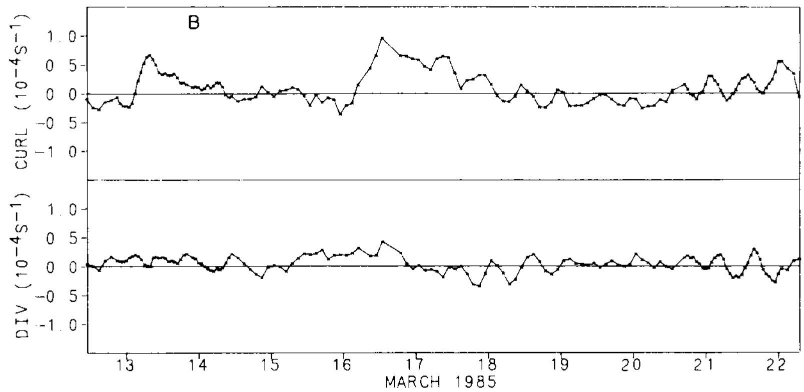

Fig. 9. Time series of curl and divergence at position B of Fig. 1.

surements, the averaging radius around the considered position had to be extended from 3 km (as for the presented two-dimensional current velocities) to 8 km. The errors of both the curl and divergence turned out to be less than $0.03 \cdot 10^{-4}$ s^{-1}, indicating that the data presented in Fig. 9 are true. Some more evidence in support of this statement follow from the continuous behaviour of the time series (of independent measurements). At other positions, the data do not look good. A number of flyers occur, usually accompanied by higher errors.

The time series of curl and divergence are hard to interpret. As may be expected from the current fields, they show some variability with position (not shown here). In Fig. 9 (upper panel), the eddy period on 16–17 March is clearly visible in the time series of the curl. There is no such period of exceptional strong divergence. But during 15–16 March, upwelling dominates. Both, the curl and divergence are present during the whole experiment and change sign several times. Starting on 18 March, both time series contain a semidiurnal component, obviously related to tides. There seems to be a 90° phase shift between curl and divergence. A comparison of tidal surface elevation, as obtained from tidal tables, and measured divergence show the time series to be in phase. This contradicts the assumption of measured divergence being due to tidal sea-level fluctuations. In fact, a rough estimation shows that the magnitude of the observed divergence may neither be explained by this assumption.

Assuming up- and downwelling, we may estimate vertical current velocities. For this purpose, we consider a simple model of an upper layer of constant divergence. Within this layer, vertical velocities become,

$$u_z = \text{div}\, \boldsymbol{u} \cdot z \tag{4}$$

with,

u_z = vertical current velocity
z = water depth.

Current meter measurements in March 1976 close to Utsira (Furnes and Saelen, 1977) show a correlation of horizontal currents down to several 10 m. Considering a layer depth of this order, the vertical velocities turn out to be less than 0.1 cm s^{-1}. It should be mentioned that this is a mean value within a circle of 8 km around the considered grid point. As Fig. 4 shows, there is some variability on this scale and locally, higher vertical velocities are possible.

Fig. 10 compares the absolute value of the nonlinear (horizontal) acceleration, as defined in Eq. 3, and the absolute value of the linear (temporal) acceleration, as given by,

$$\boldsymbol{b}_t = \left(\frac{\partial u_x}{\partial t}, \frac{\partial u_y}{\partial t} \right). \tag{5}$$

For a special time, the temporal acceleration is computed from the preceding and the following measurement. Thus, the considered time interval is twice the sampling rate and not always the same, due to different sampling rates and lacking data. Though the time series looks reasonable, the temporal acceleration may be perturbed by numerical instabilities and should be regarded

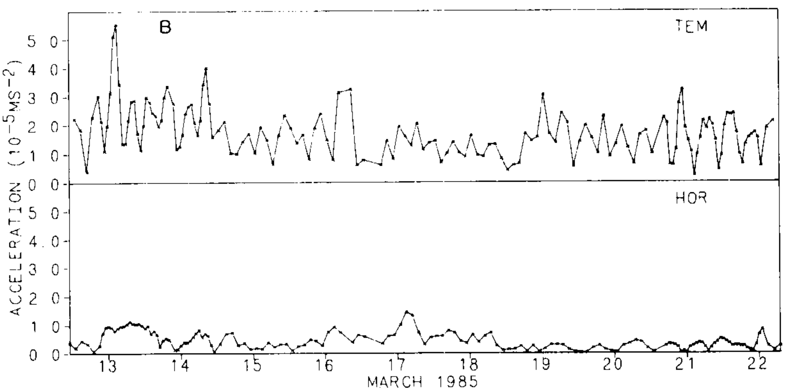

Fig. 10. Comparison of the linear temporal (TEM) and nonlinear horizontal (HOR) acceleration at position B of Fig. 1.

with some caution. The presented data refer to position B of Fig. 1, where an optimal data set is available. The horizontal acceleration is computed using the same procedures as curl and divergence (cf. Fig. 9).

The time series of the temporal acceleration are strongly affected by the semidiurnal tide, which occurs with half the period within the absolute value. There is no such dependence for the horizontal acceleration. With respect to the tidal currents, the linear acceleration considerably exceeds the nonlinear, and linear numerical models may be sufficient for this process. But in general, this is not the case. Mesoscale currents should be described by nonlinear models. From our data, a statement for large-scale processes is not possible. Moreover, in the respective models, nonlinear mesoscale processes are taken into consideration by means of parametrisation.

7. Conclusions

CODAR is the only method to measure current velocities and their horizontal derivatives in the upper 1 m of the ocean. The data presented show the high mesoscale spatial and temporal variation of currents within the Norwegian coastal current, which considerably exceeds the variability as we had observed during CODAR experiments in the southern North Sea (Janopaul et al., 1982; Essen et al., 1984) or in the Baltic (Gurgel et al., 1986). The data of current velocities may help to interpret satellite images from the Norwegian coastal current, containing no information on current velocities.

The analysis of time series at selected positions confirms the knowledge about tidal currents in the measuring area, and yields reliable ratios of current-to-wind speed, different for the north- and east-components. The analysis also shows how mesoscale processes, like a stationary eddy, may perturb the estimation of residual currents from single-point measurements. New are the results derived from the horizontal derivatives such as curl, divergence and the nonlinear acceleration, as compared with the linear. No simple explanation of these data is possible, because the currents in the measuring area are influenced by a number of different forces. The data may help modellers in developing mesoscale models or in parametrizising mesoscale processes in large-scale models.

8. Acknowledgements

We thank our colleagues R. Cordlandwehr, T. Freygang and M. Hamann, who helped to prepare and perform the experiment. We are grateful to Dr. G. K. Furnes and O. Olsen from the Geophysical Institute in Bergen for their support in logistics. The Norwegian Meteorological Institute supplied us with the wind data. This work was supported by the German Science Foundation (DFG, SFB 94).

REFERENCES

Audunson, T., Dalen, V., Krogstad, H., Lie, H. N. and Steinbakke, O. 1981. Some observations of ocean fronts, waves and currents along the Norwegian coast from satellite images and drifting buoys. In: *The Norwegian coastal current, vol. I* (ed. R. Saetre and M. Mork). Bergen: University of Bergen, 20–56.

Barrick, D. E., Evans, M. W. and Weber, B. L. 1977. Ocean surface currents mapped by radar. *Science 198*, 138–144.

Carstens, T., McClimans, T. A. and Nilsen, J. H. 1984. Satellite imagery of boundary currents. In: *Remote sensing of shelf-sea hydrodynamics* (ed. J. C. J. Nihoul). Amsterdam: Elsevier Oceanography Series, 235–256.

Davies, A. M. and Furnes, G. K. 1980. Observed and computed M2 tidal currents in the North Sea. *J. Phys. Ocean. 10*, 978–984.

Davies, A. M. and Heaps, N. S. 1980. Influences of the Norwegian Trench on the wind-driven circulation in the North Sea. *Tellus 32*, 164–175.

Davies, A. M. 1985. A three dimensional modal model of wind induced flow in a sea region. *Prog. Oceanog. 15*, 71–128, 1985.

Dooley, H. D. and Furnes, G. K. 1981. Influence of the wind field on the transport of the northern North Sea. In: *The Norwegian coastal current, vol. I* (ed. R. Saetre and M. Mork). Bergen: University of Bergen, 57–71.

Furnes, G. K. and Saelen, O. H. 1977. Currents and hydrography in the Norwegian coastal current off Utsira during JONSDAP-76. *Report 2/77*, University of Bergen, Norway.

Furness, G. K., Hackett, B. and Saetre, R. 1986. Retroflection of Atlantic water in the Norwegian Trench. *Deep-Sea Res. 3*, 247–265.

Essen, H.-H., Gurgel, K.-W. and Schirmer, F. 1983. Tidal and wind-driven parts of surface currents as measured by radar. *Dt. hydrogr. Z. 36*, 81–96.

Essen, H.-H., Freygang, T., Gurgel, K.-W. and Schirmer, F. 1984. Surface currents in front of Sylt—radar measurements in fall 1983—(in German). *Dt. hydrogr. Z. 37*, 201–215.

Gurgel, K.-W., Essen, H.-H. and Schirmer, F. 1986. CODAR in Germany—a status report valid November 1985—. *IEEE J. Oceanic Engineering, OE-11*, 251–257.

Janopaul, M. M., Broche, P., DeMaistre, J. C., Essen, H.-H., Blanchet, C., Grau, G. and Mittelstaedt, E. 1982. Comparison of measurements of sea currents by HF radar and by conventional means. *Intern. J. Remote Sens. 3*, 409–422.

Johannessen, O. M., Johannessen, J. A. and Farrelly, B. A. 1983. Application of remote sensing for studies, mapping and forecasting of eddies on the Norwegian continental shelf. *ESA SP-188*, 179–187.

McClimans, T. A. and Lonseth, L. 1985. Oscillations of frontal currents. Continent. *Shelf Res. 4*, 699–707.

Pond, S. and Pickard, G. L. 1978. *Introductory dynamic oceanography*. Oxford: Pergamon Press, 241 pp.

Vigner, A., McClimans, T. A. and Tryggestad, S., 1981. Laboratory observations of instabilities in a straight coastal current. In: *The Norwegian coastal current, vol. II* (ed. R. Saetre and M. Mork). Bergen: University of Bergen, 553–582.